https://doi.org/10.1016/j.jsv.2020.115734

Nonlinear pseudo-force in a breathing crack to generate harmonics

Wei Xu[a, b], Zhongqing Su[b], Maciej Radzieński[c],

Maosen Cao[a, d, *], Wiesław Ostachowicz[c]

[a] Department of Engineering Mechanics, Hohai University, Nanjing 210098, People's Republic of China

[b] Department of Mechanical Engineering, The Hong Kong Polytechnic University, Hung Hom, Kowloon, Hong Kong, People's Republic of China

[c] Institute of Fluid-Flow Machinery, Polish Academy of Sciences, Gdańsk 80-231, Poland

[d] Jiangxi Provincial Key Laboratory of Environmental Geotechnical Engineering and Disaster Control, Jiangxi University of Science and Technology, Ganzhou 341000, People's Republic of China

[*]Corresponding author.

E-mail addresses: wxu@hhu.edu.cn, weixu@polyu.edu.hk (W. Xu); zhongqing.su@polyu.edu.hk (Z. Su); maciej.radzienski@imp.gda.pl (M. Radzieński); cmszhy@hhu.edu.cn (M. Cao); wieslaw.ostachowicz@imp.gda.pl (W. Ostachowicz)

Abstract: A fatigue crack that periodically opens and closes subject to a harmonic excitation can be referred to as a breathing crack. Higher harmonics generated by breathing cracks can manifest the occurrence of a crack. Although the modulation due to the opening–closing motion has been widely recognized as the cause of higher harmonics, the intrinsic force that drives a breathing crack to generate harmonics is not yet clear. With the objective of providing physical insights into the intrinsic force that generates harmonics, a novel concept of nonlinear pseudo-force (NPF) in the breathing crack is proposed in this study. The NPF is analytically formulated by rearranging the equation of transverse motion of a beam bearing a breathing crack, whose bending stiffness changes periodically during forced harmonic vibration. In a physical sense, the mechanism for generating higher harmonics is explicitly expounded using the NPF. As well, the amplification effect of higher harmonics owing to differentiation is quantitatively investigated using multiple scenarios. The nonlinear behaviors of harmonics generated by breathing cracks are well explained using the NPF proposed in this study. A beam that bears a fatigue crack is taken as a specimen for experimental validation, whose steady-state velocity responses are acquired through non-contact measurement of vibration. Finally, the application potential of the NPF for detecting and locating breathing cracks is explored. In particular, this study proposes a novel nonlinear approach for crack identification using the NPF, whose capability in detecting and locating breathing cracks is verified on beams with breathing cracks.

***Keywords*:** fatigue crack; breathing crack; harmonics; nonlinear pseudo-force; non-contact measurement; crack identification

1 Introduction

Fatigue cracks can occur in structural components after long-term cyclic loads and can develop to significant degrees, jeopardizing structural integrity and safety, inducing structural failures [1]. Compared with the dimensions of a cracked structural component, the width of its fatigue crack can be negligible. Therefore, fatigue cracks can barely cause noticeable changes in the dynamic characteristics of cracked structural components. Nevertheless, fatigue cracks can open and close during tension and compression subject to cyclic loads. Such cracks are referred to as breathing cracks, whereby higher harmonics are generated to manifest the occurrence of fatigue cracks [2].

To accurately depict the opening–closing motion of a breathing crack subject to a harmonic excitation, the structural stiffness at the crack location is assumed to be instantaneous and nonlinear [2]. Clearly, superior to an open crack, this more realistic modeling manner of breathing cracks leads to nonlinear vibration responses caused by the contact of crack interfaces, in the frequency spectra of which higher harmonics at successive multiples of excitation frequencies appear. In the field of nondestructive testing (NDT), these higher harmonics can be sensitive indicators of the occurrence of fatigue cracks. Approaches relying on higher harmonics have been developed in the recent decade and have proven effectiveness in detecting fatigue cracks [3-11]. Although the modulation due to the opening–closing motion has been widely recognized as the cause of higher harmonics [5,7], explicit revelation of the mechanism for generating harmonics is a fundamental issue in investigating breathing cracks and has attracted increasing attention in the field of NDT. Advances in modeling approaches for breathing cracks and mechanisms for generating higher

harmonics were summarized in Ref. [12], providing valuable insights into their application in NDT.

In the early research into breathing cracks, cracked beams were simplified as single degree of freedom (DOF) oscillators, whose stiffness in half-cycles for tension and compression were represented by asymmetric linear or nonlinear functions [13-22]. This manner of modeling breathing cracks is reasonable because it reflects the gradual closure of cracks during vibration. Extended to cracked structures with multiple DOFs, periodical changes in crack locations have been introduced into dynamic stiffness matrices to model breathing cracks [23-30]. For continuous cracked beams with infinite DOFs, breathing cracks have been analytically modeled [31-36]. Representative studies follow. Shen and Chu [31] modeled a breathing crack that opens and closes according to the sign of the normal strain near the crack tip. A bilinear equation was formulated by a Galerkin procedure and solved numerically. Chasalevris and Papadopoulos [32] established the equation of motion of a continuous shaft with a transverse breathing crack, following the theory of Rayleigh. The crack was analytically modeled by introducing the crack compliance variance. Caddemi *et al*. [33] used a switching crack model that is similar to the breathing crack model but has only fully open and closed statuses. The nonlinear dynamic responses of Euler–Bernoulli beams with arbitrary numbers of cracks were obtained. Rezaee and Hassannejad [34] considered that local stiffness changes at the location of a breathing crack can be represented by a nonlinear amplitude-dependent function during one half-cycle of the opening–closing motion. Lim *et al*. [35] provided a physical insight into the binding conditions for nonlinear ultrasonic generation considering both propagating waves and stationary vibrations, which was experimentally validated with a special focus on the nonlinear modulation produced by a fatigue crack. Wang *et al*.

[36] developed a two-dimensional analytical model for interpreting the modulation mechanism of a breathing crack on guided ultrasonic waves. The model is capable of analytically depicting the propagating and evanescent waves induced owing to the interaction of waves with the crack.

Despite considerable efforts addressing the modeling of breathing cracks, the intrinsic force that drives a breathing crack to generate harmonics is not yet clear. Addressing this problem, the objective of this study is to analytically formulate the crack-induced force in a breathing crack, on which basis the mechanism for generating higher harmonics can be explicitly expounded. This mechanism can be a valuable supplement to existing classical theories [12]. To this end, a novel concept of nonlinear pseudo-force (NPF) in a breathing crack is proposed and analytically formulated by rearranging the equation of transverse motion of the cracked beam, by which the mechanism for generating harmonics in the breathing crack is explicitly expounded. As well, the amplification effect of higher harmonics owing to differentiation is quantitatively investigated using multiple scenarios. The nonlinear behaviors of harmonics generated by breathing cracks are well explained using the NPF proposed in this study. Finally, the application potential of the NPF for detecting and locating breathing cracks is explored. In particular, this study proposes a novel nonlinear approach for crack identification using the NPF.

It is noteworthy that contacts in crack interfaces are very complex in real cracks. Numerical approaches are commonly used to calculate nonlinear vibrations of cracked beams. However, contact parameters for crack interfaces are usually unknown and must be estimated *a priori*, which can induce non-negligible effects on the amplitudes of higher harmonics. With this concern, in this study, experiments are employed rather

than numerical simulations to quantitatively investigate the nonlinear behaviors of harmonics generated by breathing cracks.

The rest of this paper is organized as follows. Section 2 proposes and analytically formulates the concept of NPF in a breathing crack, on which basis the mechanism of generating harmonics is explicitly expounded. By using multiple scenarios, the amplification effect of higher harmonics is quantitatively investigated. Moreover, the NPF is used to explain the nonlinear behaviors of harmonics generated by breathing cracks. Section 3 experimentally validates the harmonics generated by the NPF and their nonlinear behaviors. Steady-state velocity responses of a steel cracked beam are acquired through non-contact measurement of vibration using a Doppler laser vibrometer. Section 4 proposes a novel crack localization approach using the NPF, with the application potential for detecting and locating breathing cracks explored by numerical simulations. Section 5 presents concluding remarks.

2 Harmonics generated by a breathing crack

In a uniform intact Euler–Bernoulli beam subject to a transverse excitation, its equation of transverse motion can be expressed as [37]

$$EI\frac{\partial^4 w}{\partial x^4}+\rho A\frac{\partial^2 w}{\partial t^2}+c\frac{\partial w}{\partial t}=f, \tag{1}$$

where $w(x,t)$ is the transverse displacement, x is the abscissa along the beam length, t is time, ρ is the material density, c is the damping coefficient, $f(x,t)$ is the transverse excitation, I and A are the inertia moment and area of the cross-section, respectively.

2.1 Linear pseudo-force

Assuming that a through-width notch is introduced into the beam, spanning from $x = x_1$ to $x = x_2$ in a narrow section along the beam length, its inertia moment and area of the cross-section can be represented as

$$I(x) = \begin{cases} I^I & x \notin [x_1, x_2] \\ I^N(x) & x \in [x_1, x_2] \end{cases}, \tag{2a}$$

$$A(x) = \begin{cases} A^I & x \notin [x_1, x_2] \\ A^N(x) & x \in [x_1, x_2] \end{cases}, \tag{2b}$$

where I^I and A^I are the inertia moment and area of the cross-section in the intact region, respectively, and $I^N(x)$ and $A^N(x)$ are the inertia moment and area of the cross-section within the notch section, respectively. Note that $I^N(x)$ and $A^N(x)$ are associated with varying height $h^N(x)$.

By substituting Eq. (2) into Eq. (1) and rearranging Eq. (1), we have

$$EI^I \frac{\partial^4 w}{\partial x^4} + \rho A \frac{\partial^2 w}{\partial t^2} + c \frac{\partial w}{\partial t} = f + f_{LPF}, \tag{3}$$

where $f_{LPF}(x,t)$ denotes the linear pseudo-force (LPF) that is the equivalent force caused by the notch, applying on the notch spanning from $x = x_1$ to $x = x_2$ along the beam:

$$f_{LPF} = \begin{cases} 0 & x \notin [x_1, x_2] \\ E[I^I - I^N(x)] \frac{\partial^4 w}{\partial x^4} + \rho [A^I - A^N(x)] \frac{\partial^2 w}{\partial t^2} & x \in [x_1, x_2] \end{cases}, \tag{4}$$

Equation (3) indicates that the forced vibration of the beam that bears a notch is equivalent to the vibration of an intact beam subject to the combined excitation of the external excitation and the LPF, as illustrated in Fig. 1. Because the LPF reflects the damage-caused perturbation in equilibrium of a structural element, structural damage

identification approaches using LPFs have been widely reported [38-49]: Eq. (4) indicates that the LPF appears within the notch section only and vanishes elsewhere, by which phenomenon the occurrence and location of the notch can be determined.

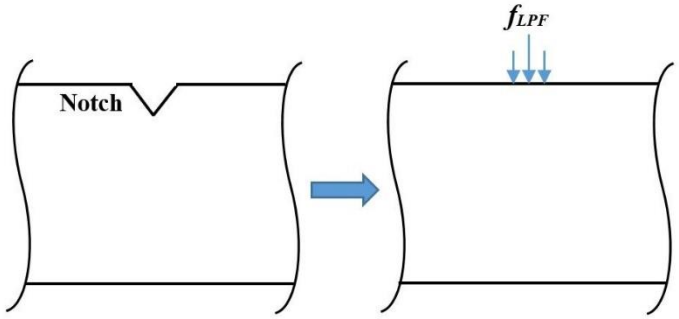

Fig. 1. Schematic of the LPF applying on a structural element with a notch.

As per linear vibration theory, when the beam is excited by an external harmonic excitation f at the frequency of ω_f, its steady-state transverse displacement w can be expressed as a monomeric harmonic wave:

$$w(x,t) = W_1(x)\cos(\omega_1 t + \phi_1), \tag{5}$$

where W_1, ω_1 ($\omega_1 = \omega_f$), and ϕ_1 denote the vibration shape of the beam, angular frequency, and phase associated with the first harmonic. Substituting Eq. (5) into Eq. (4), the LPF within the notch section can be expressed as

$$f_{LPF} = \begin{cases} 0 & x \notin [x_1, x_2] \\ E[I^I - I^N(x)]\dfrac{\mathrm{d}^4 W_1}{\mathrm{d}x^4}\cos(\omega_1 t + \phi_1) - \rho\omega_1^2[A^I - A^N(x)]W_1\cos(\omega_1 t + \phi_1) & x \in [x_1, x_2] \end{cases}. \tag{6}$$

Equation (6) indicates that the frequency of the LPF corresponds to the external excitation frequency:

$$f_{LPF}(x,t)\big|_{x\in[x_1,x_2]} = F_{LPF}(x)\cos(\omega_1 t + \phi_1), \tag{7}$$

where F_{LPF} denotes the amplitude of f_{LPF} within the notch.

2.2 Nonlinear pseudo-force

Assume that a perpendicular fatigue crack initiates in the tip of a notch at $x = x_c$, whose width is negligible compared with the notch width. The fatigue crack can periodically open and close with external excitation as a breathing crack. By means of introducing the periodical change in the bending stiffness at the crack location, the inertia moment of the cross-section at the crack location can be expressed as [17]

$$I(x,t) = \begin{cases} I^I & x \notin [x_1, x_2] \\ I^N(x) & x \in [x_1, x_c) \cap (x_c, x_2] \\ I^C - \dfrac{1}{2}(I^C - I^O)(1+\cos\omega_B t) & x = x_c \end{cases}, \tag{8}$$

where ω_B is the breathing frequency of the crack and I^C and I^O are inertia moments of the cross-section at the crack location x_c under totally closed and open statuses of the breathing crack, respectively. The heights of the cross-section at the crack location x_c associated with I^C and I^O are denoted as h^C and h^O, respectively. Note that $I^C = I^N(x_c)$ and $h^C = h^N(x_c)$ for the fully closed status of the breathing crack; h^O is excitation-dependent because the external excitation determines the opening extent of the crack during the opening–closing motion. It is also noteworthy that for flexural vibration of the cracked beam, crack-caused change in mass can be ignored compared to change in stiffness, because the crack width is negligible compared to the crack depth.

By substituting Eq. (8) into Eq. (1) and rearranging Eq. (1), we have

$$EI^I \frac{\partial^4 w}{\partial x^4} + \rho A \frac{\partial^2 w}{\partial t^2} + c\frac{\partial w}{\partial t} = f + f_{LPF} + f_{NPF}, \tag{9}$$

where f_{NPF} is the equivalent force caused by the breathing crack, defined as the NPF in this study:

$$f_{NPF} = \begin{cases} 0 & x \neq x_c \\ \frac{1}{2}(I^C - I^O)(1+\cos\omega_B t)\frac{\partial^4 w}{\partial x^4} & x = x_c \end{cases}, \tag{10}$$

Equation (10) indicates that the NPF appears only in the notch tip at $x = x_c$ and vanishes elsewhere. The forced vibration of a beam that bears a notch and a crack is equivalent to the intact beam subject to the combined excitation of the external excitation, LPF, and NPF, as illustrated in Fig. 2. As the beam is subjected to external harmonic excitation at the frequency of ω_f, it is reasonable to assume that the breathing frequency corresponds to the excitation frequency, *i.e.*, $\omega_B = \omega_f$.

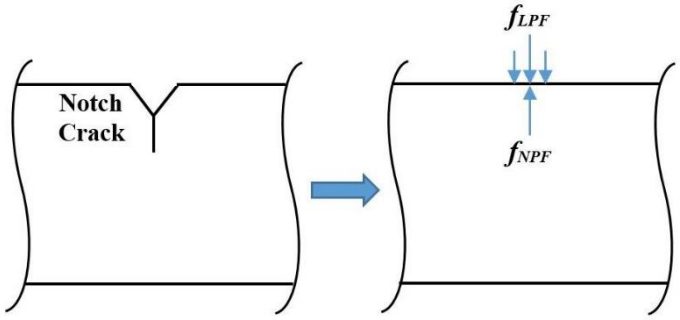

Fig. 2. Schematic of the LPF and NPF applying on a structural element that bears a notch and a crack.

The nonlinear steady-state displacement of the beam is assumed to be composed of *M* harmonics at different frequencies:

$$w(x,t) = \sum_{m=1}^{M} W_m(x)\cos(\omega_m t + \phi_m), \tag{11}$$

where W_m, ω_m, and ϕ_m denote the vibration shape of the beam, angular frequency, and phase associated with the *m*th harmonic.

Substituting Eq. (11) into Eq. (10), the NPF at $x = x_c$ can be rewritten as

$$f_{NPF}\big|_{x=x_c} = \frac{1}{2}(I^C - I^O)(1+\cos\omega_B t)\sum_{m=1}^{M}\frac{\partial^4 W_m}{\partial x^4}\cos(\omega_m t+\phi_m)$$
$$= \frac{1}{2}(I^C - I^O)\sum_{m=1}^{M}\frac{\partial^4 W_m}{\partial x^4}\cos(\omega_m t+\phi_m)(1+\cos\omega_B t) \quad (12)$$
$$= \frac{1}{2}(I^C - I^O)\sum_{m=1}^{M}\frac{\partial^4 W_m}{\partial x^4}[X_m + X_m^+ + X_m^-],$$

where term $X_m = \cos(\omega_m t+\phi_m)$ is associated with the frequency ω_m, whereas extra terms $X_m^+ = \frac{1}{2}\cos((\omega_m+\omega_B)t+\phi_m)$ and $X_m^- = \frac{1}{2}\cos((\omega_m-\omega_B)t+\phi_m)$ are associated with the side frequencies at $\omega_m+\omega_B$ and $\omega_m-\omega_B$, respectively.

In a physical sense, the LPF is produced by the notch, whereas the NPF is produced by the modulation effect induced by the breathing motion of the crack. Compared with the LPF whose frequency corresponds to the external excitation frequency, the NPF consists of components at successive multiples of the excitation frequency. Accordingly, the LPF drives linear vibrations of cracked beams, whereas the NPF drives nonlinear vibrations.

2.3 Harmonics generated by nonlinear pseudo-force

It has been widely observed that in frequency spectra, harmonics generated by breathing cracks are distributed at successive multiples of excitation frequencies. By addressing this phenomenon, some explanatory theories of stress-strain relationships have been proposed to expound mechanisms for generating harmonics [12]. By the novel concept of NPF that is proposed and analytically formulated in this study, the mechanism for generating higher harmonics can be explicitly expounded from a new perspective. As indicated in Eq. (12), the component of the NPF at ω_m is modulated by ω_B, whereby extra components at $\omega_m \pm \omega_B$ are generated. Conversely, such extra components must generate displacements at corresponding

frequencies $\omega_m \pm \omega_B$. This coupled vibration reaches a steady state and leads to the following relationship:

$$\omega_m = \omega_{m\mp 1} \pm \omega_B, \tag{13}$$

As $\omega_1 = \omega_B = \omega_f$, the solution of ω_m is easily obtained:

$$\omega_m = m\omega_f. \tag{14}$$

Equation (14) theoretically proved that higher harmonics appear at successive multiples of the excitation frequency, which is consistent with the distributions of higher harmonics observed in experiments and numerical simulations. On the other hand, the NPF in Eq. (12) can be decomposed into components at corresponding frequencies:

$$f_{NPF}\big|_{x=x_c} = \sum_{m=1}^{M} F_{NPF,m} \cos(\omega_m t + \phi_m), \tag{15}$$

where $F_{NPF,m}$ denotes the amplitude the *m*th component of f_{NPF}. It should be noted that, with the aim of revealing the mechanism for generating higher harmonics, Eq. (12) is used to expound the coupled relationship between components of the NPF and displacement, whose closed-form solution is not given in this study.

The amplification effect of higher harmonics is quantitatively investigated in this study using multiple scenarios. By differentiating the steady-state displacement w of the cracked beam in Eq. (11), the velocity v and acceleration a can be obtained:

$$v = -\sum_{m=1}^{M} W_m m\omega_f \sin(m\omega_f t + \phi_m), \tag{16a}$$

$$a = -\sum_{m=1}^{M} W_m (m\omega_f)^2 \cos(m\omega_f t + \phi_m). \tag{16b}$$

Equation (16a) indicates that each harmonic component in w is amplified by its frequency to form the corresponding component in v; similarly, Eq. (16b) indicates

that each harmonic component in v is further amplified by its frequency to form the corresponding component in a. As the second harmonics are the most sensitive to breathing cracks, the nonlinearity of a breathing crack is usually quantified by the ratios of amplitudes of the second harmonics A_2 to the amplitudes of the first harmonics A_1 [2], denoted as the nonlinearity index β:

$$\beta = \frac{A_2}{A_1}. \tag{17}$$

From Eq. (16), the amplification effect of nonlinearity indices can be found as:

$$\beta_A = 2\beta_V = 4\beta_D, \tag{18}$$

where β_D, β_V, and β_A denote the nonlinearity indices for displacements, velocities, and accelerations, respectively. It can be seen from Eq. (18) that values of the nonlinearity indices depend on response types, and can be enhanced due to the amplification effect. Compared to velocities and displacements, the amplification effect of higher harmonics causes accelerations to be more sensitive to higher harmonics. In the field of NDT, this amplification effect can be very useful for manifesting the occurrence of initial cracks, whose higher harmonics can be easily overshadowed by the first harmonics.

The nonlinear behaviors of harmonics can be well explained using the NPF, as follows. As indicated by Eq. (5), the LPF only generates the first harmonic at the excitation frequency, whereas Eq. (11) indicates that the NPF generates harmonics at successive multiples of the excitation frequency. Therefore, in a beam that bears a notch and a breathing crack, the first harmonics are determined by the external excitation, LPF, and NPF together, which means that the first harmonics are nonlinear, *i.e.*, their amplitudes show a non-proportional increase with external excitation amplitudes. Note that when the excitation is weak, the NPF is expected to be much

weaker than the LPF. In this situation, the vibration of the cracked beam is dominated by the external excitation and LPF, and can be regarded as approximately linear, almost consistent with the vibration of the beam without a fatigue crack. On the other hand, it can be seen from Eq. (12) that the NPF is associated with the difference between I^C and I^O, which depends on the opening extent of the crack during the opening–closing motion; meanwhile, the actual depth of the crack during vibration is not necessarily proportional to the amplitude of the external excitation. Therefore, the amplitudes of higher harmonics generated by the NPF can increase non-proportionally with the amplitude of the external excitation.

It is noteworthy that the NPF concept proposed in this study can be extended to other types of structural components. (i) Besides breathing cracks, damage characterized by closing–opening interfaces such as breathing delamination can also produce NPFs, which can be formulated by introducing the periodical change in bending stiffness of the delamination. (ii) In a cracked beam subjected to axial excitation, the periodical change in the cross-sectional area of the breathing crack can be introduced in its equation of longitudinal motion, whereby the axial NPF can formulated. Thereby, the coupled relationship between components of the axial NPF and longitudinal displacement can be established to expound the mechanism of generating longitudinal higher harmonics. (iii) In a cracked beam subjected to transverse vibro-acoustic excitation, following the principle in Eq. (12), the components of NPF at multiples of acoustic excitation frequency can be modulated by the components of displacement at multiples of vibration excitation frequency, whereby sideband harmonics can be generated.

3 Experimental validation

Harmonics generated by NPFs and their nonlinear behaviors are experimentally validated on a cracked steel beam subject to harmonic excitations. The beam bears a V-shaped notch, in the tip of which a fatigue crack opens and closes during steady-state vibration.

3.1 Experimental specimen and set-up

The steel beam specimen shown in Fig. 3 has the dimensions 400 mm × 10 mm × 20 mm in length, width, and thickness, respectively. One end of the beam is fixed by a vice, spanning 20 mm from the edge of the fixed end. At 92 mm from the edge of the fixed end, a through-width V-shaped notch has been manufactured from the upper surface. The notch is 1 mm deep and from the tip of which a perpendicular fatigue crack initiates and develops to the depth of 5 mm after fatigue loadings. Figure 3(a) shows the sketch of the cracked beam; a zoomed-in view of the notch and the fatigue crack is shown in Fig. 3(b).

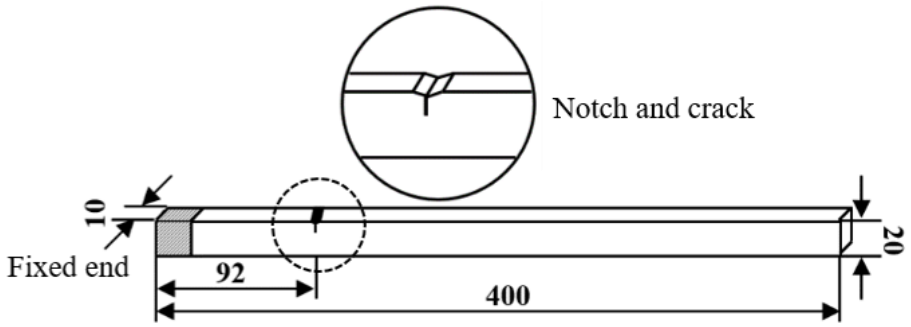

(a)

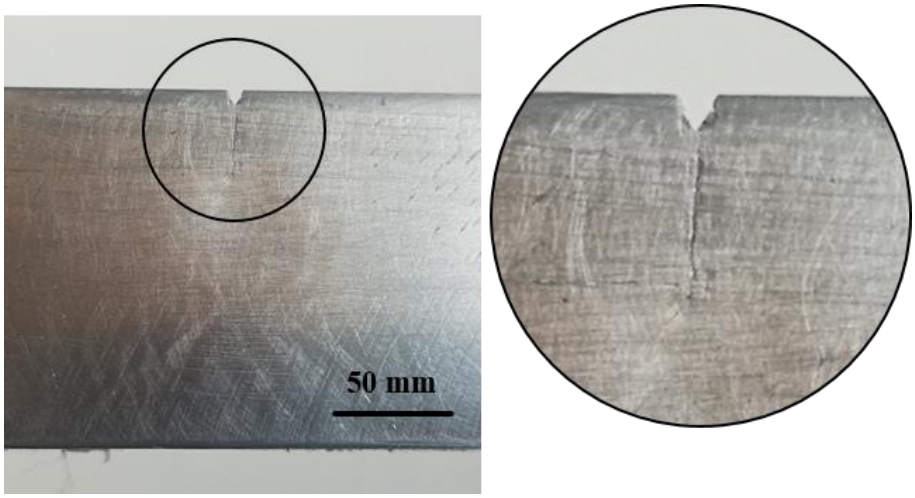

(b)

Fig. 3. Experimental specimen: (a) sketch of steel beam with a notch and a crack (dimensions in millimeters) and (b) zoomed-in view of the notch and the fatigue crack.

On the upper surface, at the location 30 mm from the edge of the fixed end, an electromechanical shaker is attached to the beam to generate pointwise harmonic forces in the transverse direction, whereby corresponding flexural harmonic vibrations of the beam can be excited. Simultaneously, velocity responses are acquired from measurement points uniformly distributed on the lower surface. After modal analysis, the first natural frequency of the beam, denoted ω_{N1}, is found to be 222.60 rad/s, *i.e.*, 70.63 Hz. The beam is excited at $1/3\,\omega_{\mathrm{N1}}$, $1/2\,\omega_{\mathrm{N1}}$, and ω_{N1}, considered as Scenarios I, II, and III, respectively. In each scenario, voltages of 0.125, 0.25, 0.5, 1, 2, and 4 V are input into the arbitrary waveform generator to control the shaker to generate proportional transverse forces. Simultaneously, the flexural steady-state velocity responses lasting 10.24 s are acquired using a non-contact Doppler laser vibrometer with the sampling frequency of 12.8 kHz. The experimental set-up (the electromechanical shaker and the Doppler laser vibrometer) are shown in Fig. 4. It should be noted that excitations with higher voltage are not considered in this study,

to exclude the effects of geometrical nonlinearity caused by large deformations. The sampling frequency of 12.8 kHz is more than enough to cover the first several higher harmonics of the beam for all the scenarios in this study.

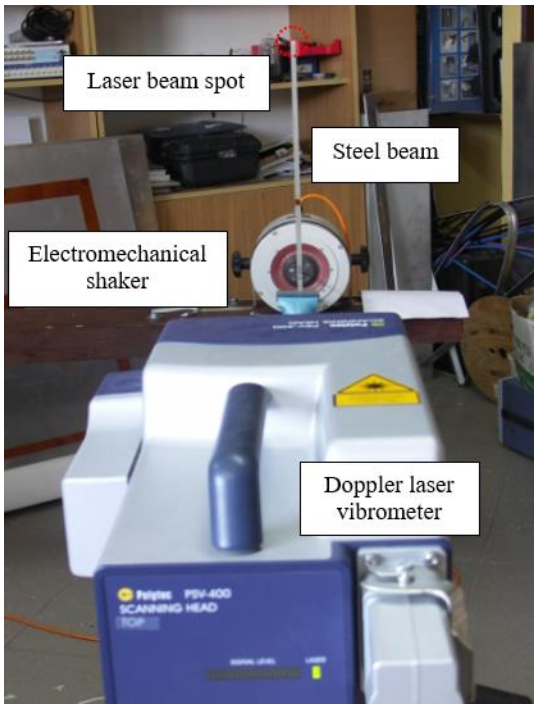

Fig. 4. Experimental set-up.

3.2 Experimental results

3.2.1 Higher harmonics generated by breathing crack

For Scenario I with the excitation voltage of 2 V, the velocity responses in the vicinity of the crack, about 94 mm from the edge of the fixed end (2 mm from the notch tip), are acquired by the Doppler laser vibrometer. Figure 5(a) shows the measured time history of the steady-state velocity response during the first two seconds. It can be seen that the velocity response approximates a monomeric harmonic wave, which means that the first harmonic is the principal component of the velocity response and dominates the steady-state vibration. The frequency spectrum of the velocity response is obtained by fast Fourier transform, as shown in Fig. 5(b). It can be seen from Fig. 5(b) that, besides the first harmonic at the excitation frequency, the second and third

harmonics with much less pronounced amplitudes appear at the frequencies of twice and thrice the excitation frequency, respectively. Thereby, harmonics are distributed at successive multiples of the excitation frequency, which correspond to the theoretical frequencies of harmonics predicted in Eq. (14).

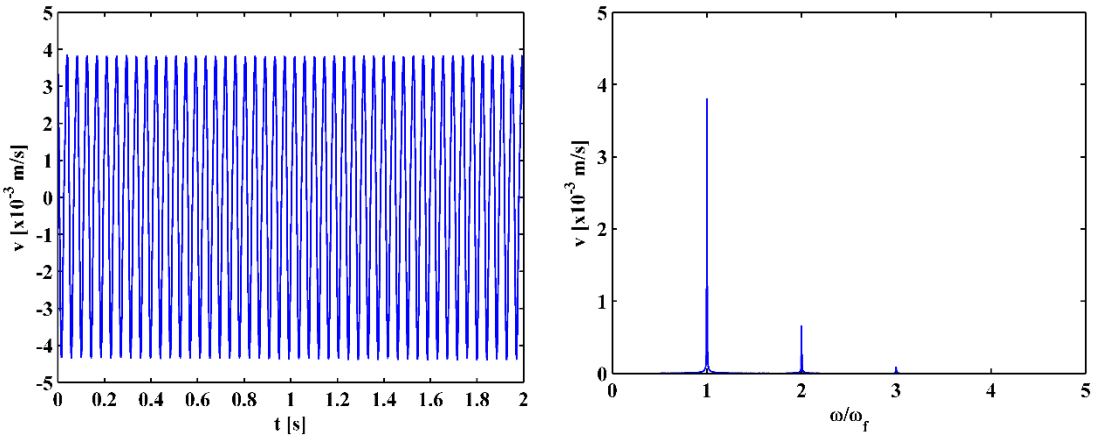

(a) (b)

Fig. 5. (a) Time history of the velocity response in the vicinity of the crack and (b) its frequency spectrum.

3.2.2 Amplification effect of higher harmonics

In real-world structural components, approximate crack locations are usually unknown; thus, for generality, responses in this study are acquired from a measurement point close to the free end of the beam (10 mm from the edge of the free end). A laser spot on the measurement point is marked in a red dotted circle, as shown in Fig. 4. The measured time history of the velocity response in the first two seconds is shown in Fig. 6(a), and Fig. 6(b) shows its frequency spectra. The nonlinearity indices of the velocity responses shown in Figs. 5(b) and 6(b) are 0.1743 and 0.2316, respectively, which means that in this case the second harmonics do not attenuate when propagating from the crack to the free end.

The acceleration response is calculated from the velocity response by the finite difference method, as shown in Fig. 7(a). Compared with the velocity response in Fig.

6(a), the acceleration response becomes much more fluctuant, clearly indicating that harmonics at higher frequencies are enhanced to a noticeable degree. From comparisons of the frequency spectra of the velocity and acceleration responses in Fig. 6(b) and 7(b), it can be seen that higher harmonics in the acceleration response are enhanced and become pronounced. This amplification effect is further quantitatively validated using Scenarios I, III, and III with the excitation voltage of 2 V. The amplitudes of the first three harmonics in velocities for the three scenarios are listed in Table 1, from which predicted accelerations (abbreviated as Pred. acc.) are obtained by Eq. (16) and calculated accelerations (abbreviated as Cal. acc.) are obtained by the finite difference method. As can be seen from Table 1, the amplitudes of the predicted and calculated harmonics are in good agreement, with negligible relative errors. Nonlinearity indices for the acceleration responses are twice of those for velocity responses, consistent with Eq. (18). Thereby, the amplification effect is quantitatively investigated using multiple scenarios, which benefits the indication of initial cracks with weak higher harmonics.

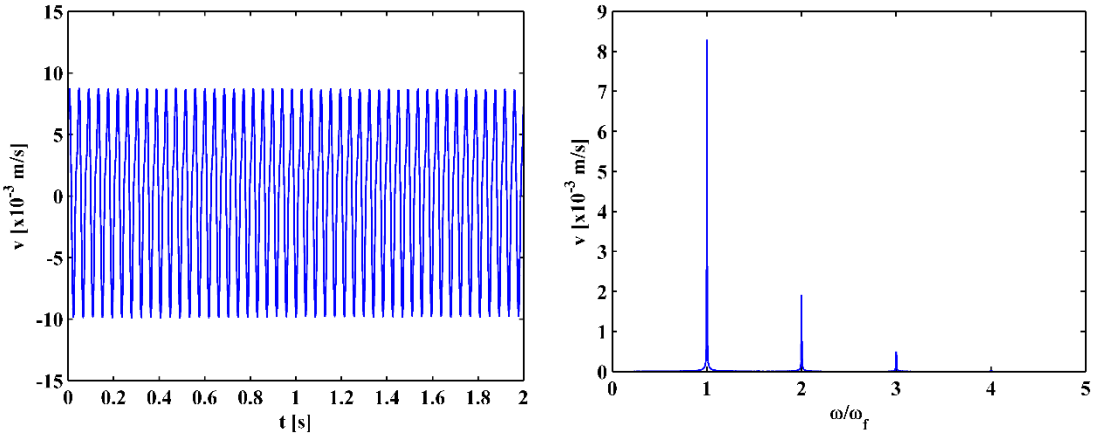

(a) (b)

Fig. 6. (a) Time history of the velocity response for Scenario I with the excitation voltage of 2 V and (b) its frequency spectrum.

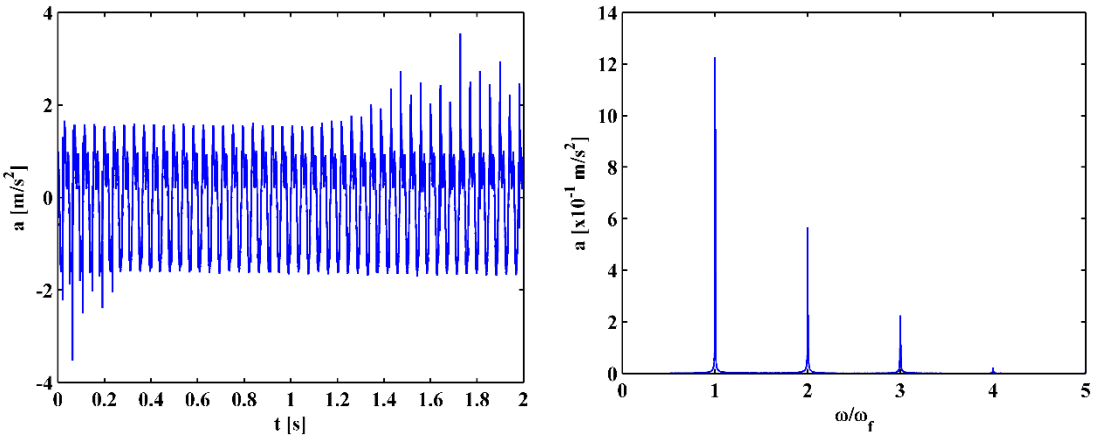

(a) (b)

Fig. 7. (a) Time history of the acceleration response for Scenario I with the excitation voltage of 2 V and (b) its frequency spectrum.

Table 1. Amplitudes of harmonics in velocities with the excitation voltage of 2 V.

Scenario	Responses and errors	The 1st harmonics	The 2nd harmonics	The 3rd harmonics	Nonlinearity indices
I	**Vel. [m/s]**	0.008289	0.001920	0.0005060	0.2316
	Pred. acc. [m/s^2]	1.2262	0.5680	0.2246	
	Cal. acc. [m/s^2]	1.2260	0.5682	0.2253	0.4635
	Error [%]	0.013933	0.027896	0.331157	
II	**Vel. [m/s]**	0.03121	0.01579	0.0009030	0.5059
	Pred. acc. [m/s^2]	6.9252	7.0073	0.6010	
	Cal. acc. [m/s^2]	6.9290	7.0090	0.5933	1.0015
	Error [%]	0.054487	0.023907	1.304014	
III	**Vel. [m/s]**	0.07471	0.001585	0.0001680	0.02121
	Pred. acc. [m/s^2]	33.1550	1.4068	0.2231	
	Cal. acc. [m/s^2]	33.1500	1.3970	0.2331	0.04214
	Error [%]	0.015036	0.700806	4.275505	

3.2.3 Nonlinear behaviors of harmonics

Amplitudes of the first and second harmonics in accelerations for Scenarios I, III, and III are listed in Table 2, from which the corresponding nonlinearity indices are obtained to quantitatively investigate the nonlinear behaviors of harmonics.

Table 2. Amplitudes of the first and second harmonics in accelerations

Scenario	Excitation voltage [V]	1st harmonic [m/s^2]/normalized		2nd harmonic [m/s^2] /normalized		Nonlinearity indices
I	**0.125**	0.07012	1	0.00176	1	0.0251
	0.25	0.1421	2.0265	0.00472	2.6818	0.0332
	0.5	0.3047	4.3454	0.02887	16.4034	0.0947
	1	0.5894	8.4056	0.1080	61.3636	0.1832
	2	1.2260	17.4843	0.5682	322.8409	0.4635
	4	2.5750	36.7228	2.1020	1194.3182	0.8163
II	**0.125**	0.7457	1	0.08579	1	0.1150
	0.25	1.7590	2.3589	0.4400	5.1288	0.2501
	0.5	4.1400	5.5518	2.6870	31.3207	0.6490
	1	5.5780	7.4802	4.6590	54.3070	0.8352
	2	6.9290	9.2919	7.0090	81.6995	1.0115
	4	7.8210	10.4881	9.1570	106.7374	1.1708
III	**0.125**	3.0640	1	0.04538	1	0.0148
	0.25	5.5960	1.8264	0.1304	2.8735	0.0233
	0.5	11.6600	3.8055	0.1878	4.1384	0.0161
	1	20.1700	6.5829	0.5535	12.1970	0.0274
	2	33.1500	10.8192	1.3970	30.7845	0.0421
	4	53.3300	17.4054	2.8720	63.2878	0.0539

In Scenario I, the acceleration responses in their frequency spectra with the excitation voltages of 0.125, 0.25, 0.5, 1, 2, and 4 V are shown in Fig. 8(a) to (f), respectively. For excitations with the low voltages of 0.125, 0.25, and 0.5 V, the opening–closing motions of the breathing fatigue crack are slight, with the result that the fatigue crack does not fully open and close with the maximum depth of 5 mm. As shown in Fig. 8(a) to (c), the second harmonics are much weaker than the first harmonics, with respective nonlinearity indices of 0.0251, 0.0332, and 0.0947. In these cases, vibrations of the cracked beam are approximately linear and dominated by the first harmonics. When the excitation voltage is increased to 1, 2, and 4 V, the second harmonics become increasingly more evident (shown in Fig. 8(d) to (f)) with increasing nonlinearity indices of 0.1832, 0.4635, and 0.8163, because the actual crack depth increases with the excitation amplitudes. Therefore, the amplitudes of higher harmonics are dependent on excitation amplitudes.

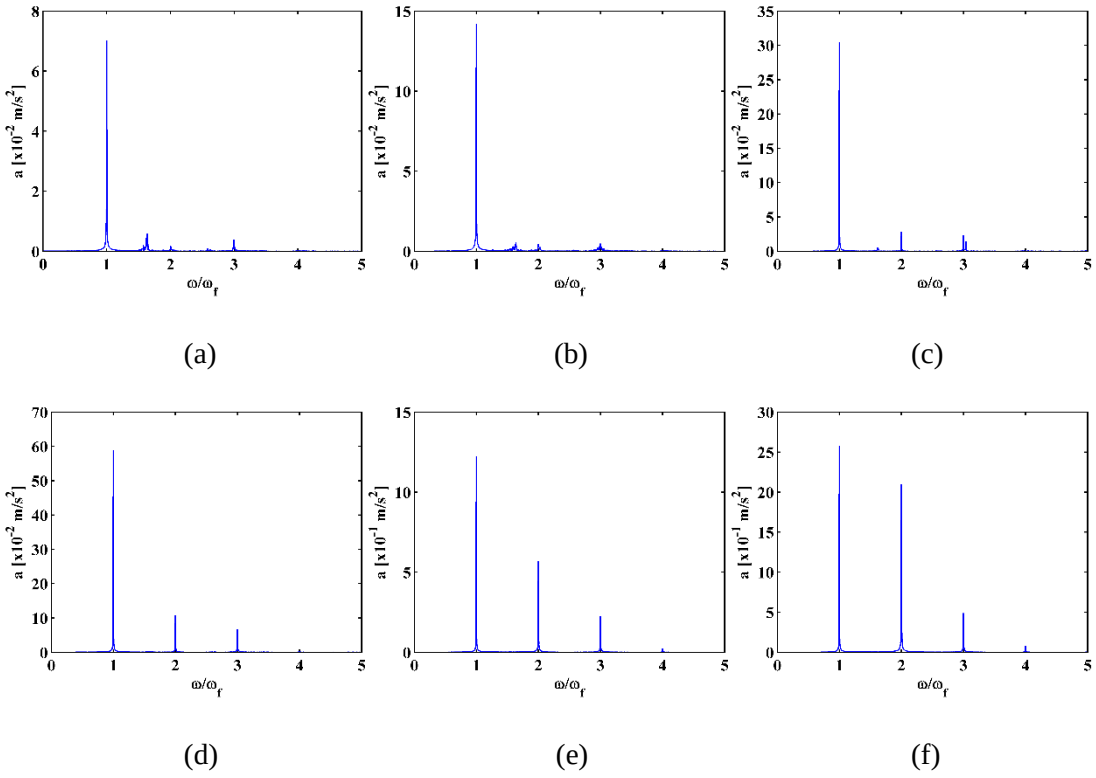

Fig. 8. Frequency spectra of acceleration responses for Scenario I with excitation voltages of (a) 0.125, (b) 0.25, (c) 0.5, (d) 1, (e) 2, and (f) 4 V.

In Scenario II, however, it can be seen from Fig. 9(a) to (d) that higher harmonics are noticeable even when subject to excitations with small voltages, whose nonlinearity indices increase from 0.1150 to 0.8352. As shown in Fig. 9(e) and (f), the second harmonics even exceed the first harmonics in amplitude, with nonlinearity indices of 1.0115 and 1.1708, when the excitation voltages increase to 2V and 4 V, respectively. In contrast, in Scenario III with excitation voltages from 0.125 to 0.5 V, the second harmonics almost vanish, with negligible nonlinearity indices, as shown in Fig. 10(a) to (c), respectively. With higher excitation voltages, the second harmonics are still much weaker, as shown in Fig. 10(d) to (f), with the maximum nonlinear index being 0.0539. In the cracked beam in this study, the higher harmonics are sensitive to the excitation frequency of $1/2\,\omega_{N1}$ but less sensitive to ω_{N1}. Therefore, the amplitudes of higher harmonics are dependent on excitation frequencies.

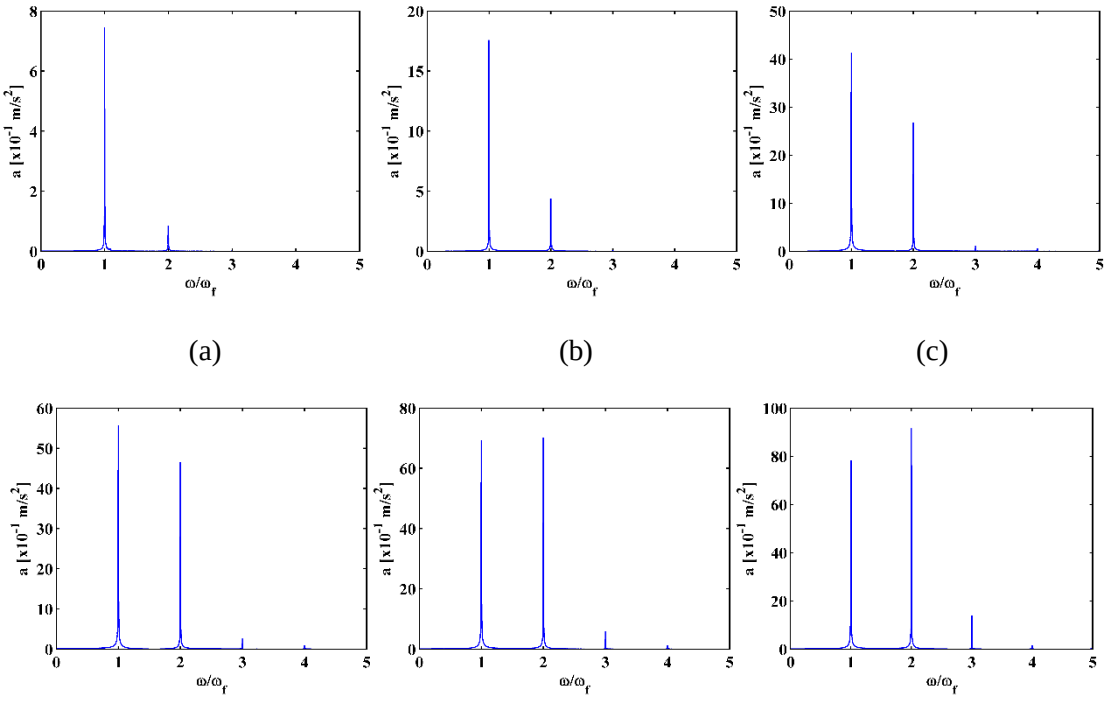

Fig. 9. Frequency spectra of acceleration responses for Scenario II with excitation voltages of (a) 0.125, (b) 0.25, (c) 0.5, (d) 1, (e) 2, and (f) 4 V.

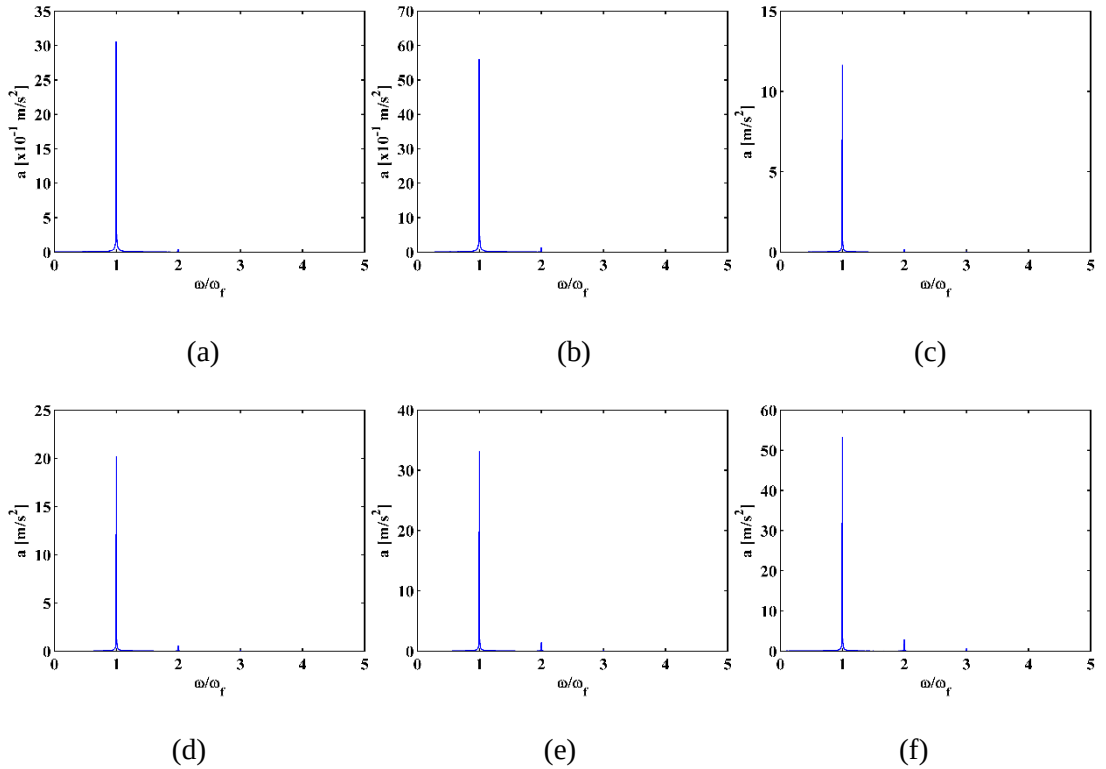

Fig. 10. Frequency spectra of acceleration responses for Scenario III with excitation voltages of (a) 0.125, (b) 0.25, (c) 0.5, (d) 1, (e) 2, and (f) 4 V.

The nonlinear behaviors of harmonics can be well explained using the NPF proposed in this study. Amplitudes of the first harmonics for each Scenario are normalized through dividing by the amplitude of the first harmonic with the smallest excitation voltage of 0.125 V. Similarly, amplitudes of the second harmonics for each Scenario are normalized. The normalized amplitudes of the first harmonics A_1 for Scenarios I, II, and III are shown in Fig. 11(a), (b), and (c), respectively. Note that the normalized A_1 are supposed to be 1, 2, 4, 8, 16, and 32 under the linear vibration assumption if the breathing crack is not considered, also shown in Fig. 11. It can be seen from Fig. 11 that when the beam is subjected to the weak excitations with small voltages, the normalized A_1 for nonlinear vibration (blue bars) are approximately proportional to the excitation amplitudes, in general agreement with the normalized A_1 for linear vibration (gray bars); when the excitation increases with higher voltages, absolute differences between normalized A_1 for nonlinear vibration and linear vibration increase more and more. This nonlinear behavior of the first harmonics can be explained using the concepts of LPF and NPF as follows. As indicated in Eq. (4), the LPFs are associated with the vibration displacement in a linear manner; in contrast, as indicated in Eq. (10), the NPFs are associated with the vibration displacement in a nonlinear manner, owing to the excitation-dependent crack depth and the modulation induced by the opening–closing motion of the crack. These increasing absolute differences between linear and nonlinear vibrations are entirely caused by the increasing NPF. When the excitation amplitudes are small, the NPF can be negligible compared with the LPF. In that situation, the vibration can be regarded as approximately linear, and the amplitudes of the first harmonics increase almost proportional to the excitation amplitudes. The actual depth of the fatigue crack increases with the excitation amplitudes, so that the first harmonics generated by the

NPF can no longer be negligible. When the excitation amplitudes are large enough, the first harmonics are partially determined by the NPF, so that their amplitudes become non-proportional to excitation amplitudes. It is noteworthy that the differences are found to be positive or negative for different excitation frequencies. Because of the directions of the external excitation, LPF and NPF can be the same or opposite, depending on excitation frequencies.

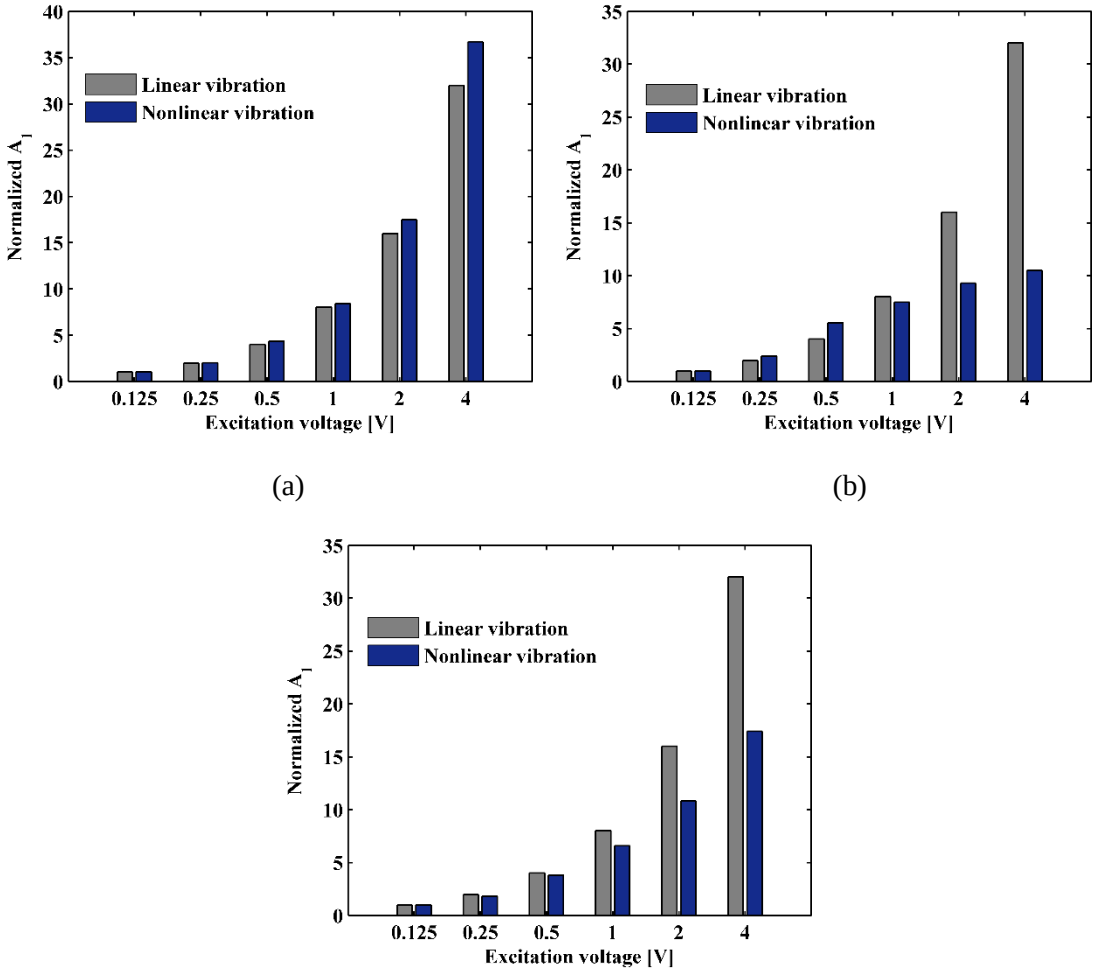

Fig. 11. Acceleration amplitudes of the first harmonics for (a) Scenario I, (b) Scenario II, and (c) Scenario III.

On the other hand, the amplitudes of higher harmonics increase non-proportionally with the amplitudes of the external excitations, because the NPF that generates higher harmonics is determined by the external excitation in a nonlinear

manner. The normalized amplitudes of the second harmonics A_2 for Scenarios I, II, and III, are shown in Fig. 12(a), (b), and (c), respectively. It can be seen from Fig. 12 that the amplitudes of the second harmonics increase rapidly with excitation voltages in Scenarios I and III; in contrast, the amplitudes of the second harmonics are less sensitive to excitation voltages in Scenario II. Thus, the second harmonics for Scenarios I ($1/3\,\omega_{N1}$) and III (ω_{N1}) are sensitive to the excitation amplitudes, whereas the second harmonics for Scenario II ($1/2\,\omega_{N1}$) are less sensitive.

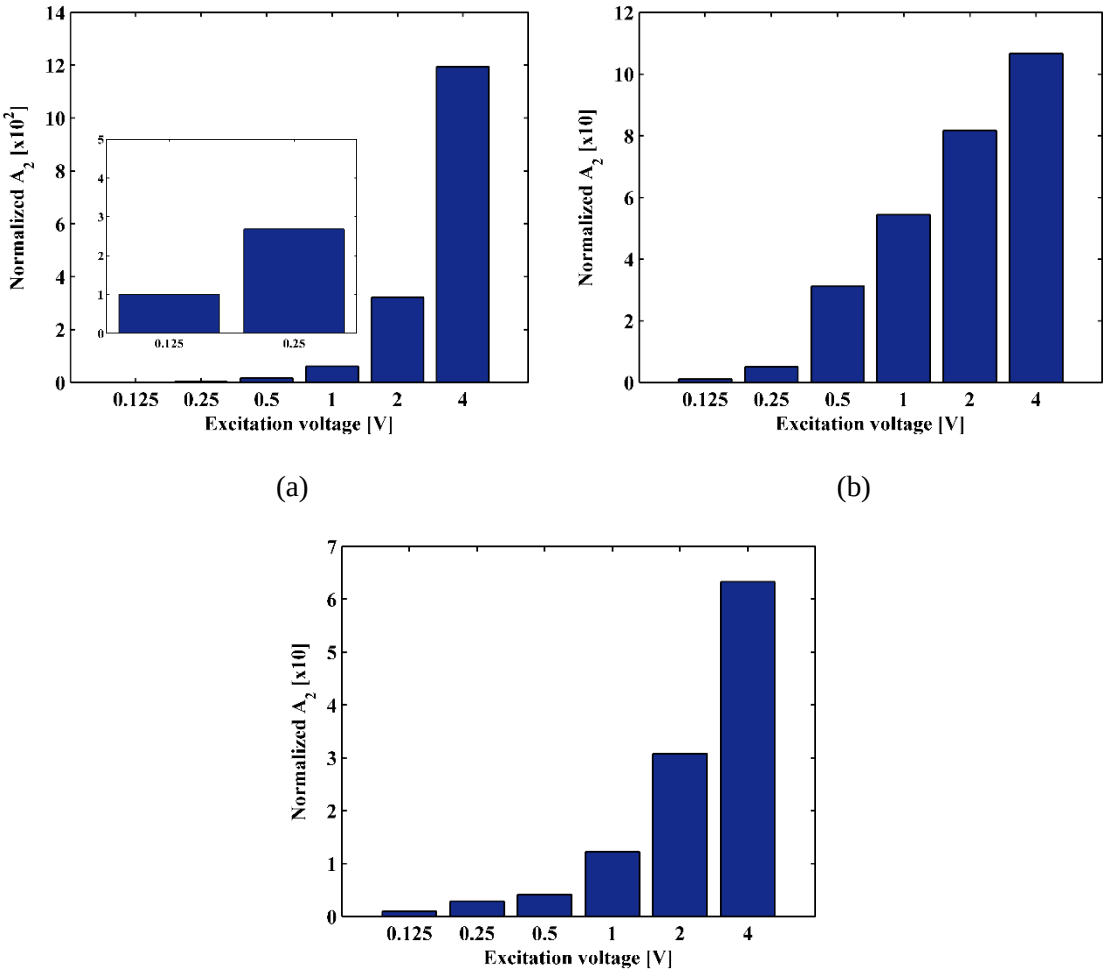

Fig. 12. Acceleration amplitudes of the second harmonics for (a) Scenario I, (b) Scenario II, and (c) Scenario III.

For applications in the field of NDT, this study provides insightful understanding of harmonics for existing fatigue crack detection approaches relying on higher harmonics: in a physical sense, the NPF can be regarded as the intrinsic force that drives a breathing crack to generate harmonics; more importantly, the NPF appears in the crack location only and vanishes elsewhere, which benefits crack detection and localization. By addressing this property of the NPF, the application potential of the NPF in detecting and locating breathing cracks is explored in the following section.

4 Crack detection and localization using NPF

In this study, a novel nonlinear approach for crack identification using the NPF is proposed, whose capability in detecting and locating breathing cracks is numerically verified using the finite element (FE) method.

Consider a lightly-damped beam that bears a notch and a breathing crack. For its elements without external excitation applied to them, one can obtain equations of motion by substituting Eqs. (7), (11), and (15) into Eq. (9):

$$F_{LPF}+F_{NPF,1}=EI^{I}\frac{\mathrm{d}^4 W_1}{\mathrm{d}x^4}+\rho A\omega^2 W_1, \tag{19a}$$

$$F_{NPF,m}=EI^{I}\frac{\mathrm{d}^4 W_m}{\mathrm{d}x^4}+\rho A(m\omega)^2 W_m, \quad m=2,3,4,... \tag{19b}$$

It can be seen from Eq. (19a) that F_{LPF} and $F_{NPF,1}$ are associated with W_1. Note that when the beam bears only a notch, the NPF associated with the first harmonic in Eq. (19a) vanishes and Eq. (19a) degenerates into the expression of the LPF:

$$F_{LPF}=EI^{I}\frac{\mathrm{d}^4 W_1}{\mathrm{d}x^4}+\rho A\omega^2 W_1. \tag{20}$$

Notch-caused perturbation in equilibrium can produce a peak in F_{LPF} to indicate the occurrence and location of the notch [38-50]. In this study, a novel nonlinear approach for crack identification is proposed using NPFs. When the beam bears only a

breathing crack, the LPF in Eq. (19a) vanishes and Eq. (19a) degenerates into the expression of the NPF associated with the first harmonic:

$$F_{NPF,1}=EI^{I}\frac{\mathrm{d}^4 W_1}{\mathrm{d}x^4}+\rho A\omega^2 W_1. \tag{21}$$

Crack-caused perturbation in equilibrium can produce a peak in $F_{NPF,1}$ that indicates the occurrence and location of the breathing crack. For higher harmonics, $F_{NPF,m}$ associated with corresponding W_m can be used for crack detection and localization as well, as expressed in Eq. (19b).

A cantilever beam with the dimensions 400 mm × 10 mm × 20 mm in length, width, and thickness, respectively is considered as the numerical specimen. The beam is modeled by the FE software ANSYS with 8-node hexahedron elements. A perpendicular breathing crack is introduced, on the interfaces of which coincident nodes in adjacent but separated elements are distributed. Contact elements are introduced between the crack interfaces. Seven scenarios are considered in this study: the crack is modeled at dimensionless abscissa ζ_c, from 0.2 to 0.8 with the interval of 0.1. In each scenario, the beam is excited by a harmonic force of 100 N at its free end to ensure that the breathing crack opens and closes totally during the steady-state vibration. As the higher harmonics are found to be less sensitive to the first natural frequency of the beam, the excitation frequency is chosen to be the first natural frequency, in order to explore the capability of the approach in detecting and locating breathing cracks. Simultaneously, steady-state acceleration responses are acquired from 41 uniformly distributed nodes on the intact surface of the beam along its length, from dimensionless abscissa ζ from 0 to 1 at intervals of 0.025.

The vibration shapes W_1 at the first harmonics are shown in Fig. 13(a) with ζ_c from 0.2 to 0.8, from which corresponding $F_{NPF,1}$ can be obtained by Eq. (21) and is shown in Fig. 13(b). It can be seen from Fig. 13(b) that, in each curve of $F_{NPF,1}$, a peak appears in the crack location. Similarly, from the vibration shapes W_2 at the second harmonics shown in Fig. 14(a), corresponding $F_{NPF,2}$ can be obtained by Eq. (19b) and are shown in Fig. 14(b), in which peaks appear in corresponding crack locations with ζ_c from 0.2 to 0.8. Thus, the breathing cracks can be detected accurately and located by both $F_{NPF,1}$ and $F_{NPF,2}$. It can be also found that in intact locations of the beam, $F_{NPF,1}$ and $F_{NPF,2}$ almost vanish, which is consistent with Eq. (10). Note that absolute values of NPFs for this approach are used for crack detection and localization.

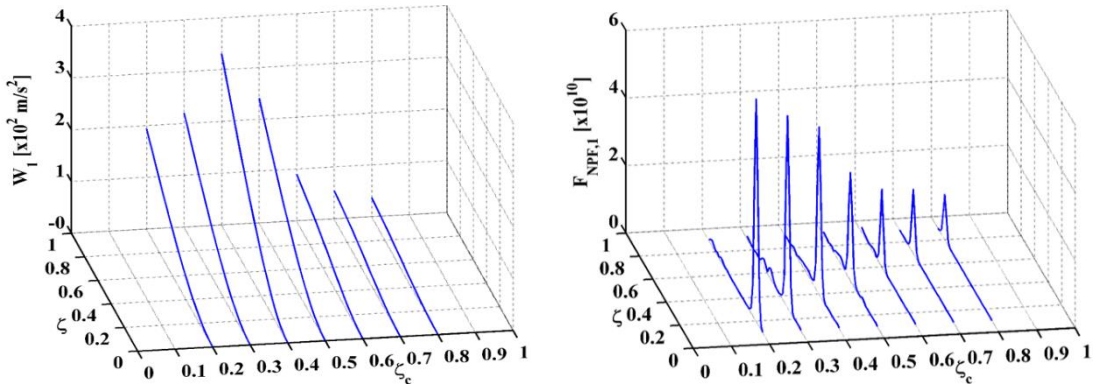

(a) (b)

Fig. 13. (a) Vibration shapes and their (b) NPFs associated with the first harmonics.

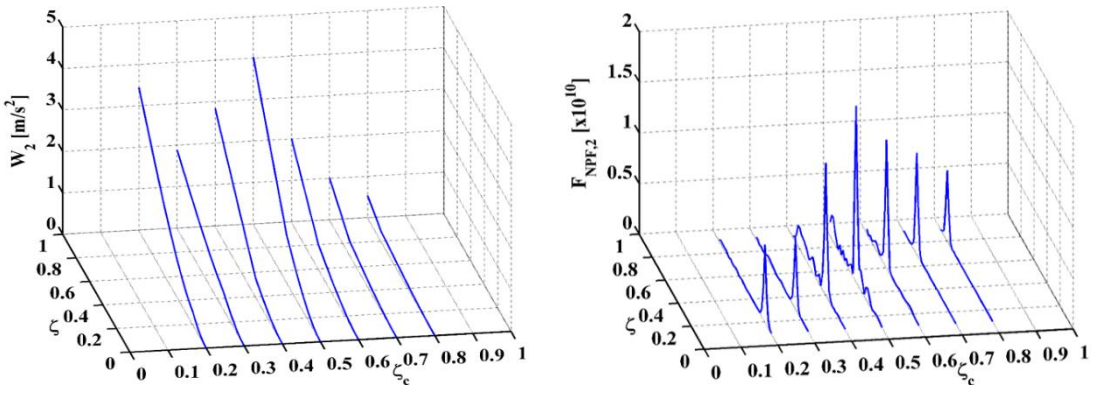

(a) (b)

Fig. 14. (a) Vibration shapes and their (b) NPFs associated with the second harmonics.

In the present study, the damage identification approach using the NPF is focused on the identification of breathing cracks. In a future study, the approach with the NPF concept can be extended to other types of damages characterized by closing–opening interfaces, such as breathing delamination, which have usually been identified by linear approaches [50-55].

5 Concluding remarks

With the objective of finding the intrinsic force that drives a breathing crack to generate harmonics, a novel concept of NPF in a breathing crack is proposed and analytically formulated in this study, on which basis the mechanism to generate higher harmonics is explicitly expounded in a physical sense. The amplification effect of higher harmonics owing to differentiation is quantitatively investigated using multiple scenarios. The nonlinear behaviors of harmonics generated by breathing cracks are well explained using the NPF and are experimentally validated on a beam bearing a fatigue crack through non-contact vibration measurement. Finally, the application potential of the NPF for detecting and locating breathing cracks is explored. Some conclusions are drawn as follows.

(1) During the opening–closing motion of a breathing crack, due to the modulation induced by the periodical change in its bending stiffness, the NPF generates extra components at side frequencies. Conversely, such extra components generate displacements at corresponding frequencies. This coupled vibration reaches a steady state, whereby harmonics at successive multiples of the excitation frequency are generated.

(2) By differentiating displacement responses, harmonics in displacements are amplified in velocities. Harmonics at higher frequencies are amplified with greater amplitudes. Similarly, these harmonics can be further amplified in accelerations. In the field of NDT, this principle can be very useful for identifying damage-caused weak higher harmonics, which can be easily overshadowed by the first harmonics.

(3) The first harmonic is generated by the external excitation, LPF, and NPF together, and its amplitude can non-proportionally increase with the amplitude of the external excitation. When the excitation has small amplitude, the NPF can be negligible compared with the LPF. Then, the vibration of the cracked beam can be regarded as approximately linear, consistent with vibration of the beam without a fatigue crack.

(4) Higher harmonics are entirely generated by the NPF, and are excitation-dependent. Excitation amplitudes and frequencies have noticeable effects on the amplitudes of higher harmonics. Those amplitudes increase with the excitation amplitude in a non-proportional manner. On the other hand, the opening–closing motions of breathing fatigue cracks depend on excitation frequencies, leading to higher harmonics sensitive to certain excitation frequencies and less sensitive to others.

(5) A novel crack localization approach using the NPF is proposed. As the NPF appears in the location of a breathing crack and vanishes elsewhere, it can be applied to detect and locate the crack using structural vibration shapes. A peak in the absolute

value of NPF can indicate the occurrence and location of a breathing crack. Applications of the NPF in detection, localization, and quantitative evaluation of breathing cracks in real-world complex structures through non-contact vibration measurement techniques such as digital imaging and laser scanning can be addressed in a future study.

Acknowledgments

This work is supported by the National Key R&D Program of China (No. 2018YFF0214705). Maosen Cao and Zhongqing Su are grateful for the support from the National Natural Science Foundation of China through Grant Nos. 11772115 and 51875492, respectively. This work is also partially supported by the Natural Science Foundation of Jiangsu Province (No. BK20171439). Dr. Xu is particularly grateful for the fellowship provided by the Hong Kong Scholars Program (No. XJ2018042).

References:

[1] A. Israr, M. Cartmell, E. Manoach, I. Trendafilova, W. Ostachowicz, M. Krawczuk, A. Żak, Analytical modeling and vibration analysis of partially cracked rectangular plates with different boundary conditions and loading, *Journal of Applied Mechanics*, 76(1) (2009) 011005.

[2] A. Bovsunovsky, C. Surace, Non-linearities in the vibrations of elastic structures with a closing crack: A state of the art review, *Mechanical Systems and Signal Processing*, 62-63 (2015) 129–148.

[3] F. Semperlotti, K. Wang, E. Smith, Localization of a breathing crack using nonlinear subharmonic response signals, *Applied Physics Letters*, 95(25) (2009) 254101.

[4] F. Semperlotti, K. Wang, E. Smith, Localization of a breathing crack using super-harmonic signals due to system nonlinearity, *AIAA Journal*, 47(9) (2009) 2076–2086.

[5] H. Hu, W. Staszewski, N. Hu, R. Jenal, G. Qin, Crack detection using nonlinear acoustics and piezoceramic transducers—instantaneous amplitude and frequency analysis, *Smart Materials and Structures*, 19(6) (2010) 065017.

[6] G. Kim, D. Johnson, F. Semperlotti, K. Wang, Localization of breathing cracks using combination tone nonlinear response, *Smart Materials and Structures*, 20(5) (2011) 055014.

[7] A. Klepka, W. Staszewski, R. Jenal, M. Szwedo, J. Iwaniec, T. Uhl. Nonlinear acoustics for fatigue crack detection—experimental investigations of

vibro-acoustic wave modulations, *Structural Health Monitoring-An International Journal*, 11(2) (2011) 197–211.

[8] E. Asnaashari, J. Sinha, Development of residual operational deflection shape for crack detection in structures, *Mechanical Systems and Signal Processing*, 43(1-2) (2014) 113–123.

[9] D. Broda, L. Pieczonka, V. Hiwarkar, W.J. Staszewski V.V. Silberschmidt, Generation of higher harmonics in longitudinal vibration of beams with breathing cracks, *Journal of Sound and Vibration*, 381 (2016) 206–219.

[10] Z. Lu, D. Dong, H. Ouyang, S. Cao, C. Hua, Localization of breathing cracks in stepped rotors using super-harmonic characteristic deflection shapes based on singular value decomposition in frequency domain, *Fatigue and Fracture of Engineering Materials and Structures*, 40 (2017) 1825–1837.

[11] K. Wang, Z. Fan, Z. Su, Orienting fatigue cracks using contact acoustic nonlinearity in scattered plate waves, *Smart Materials and Structures*, 27 (2018) 09LT01.

[12] T. Kundu, Nonlinear Ultrasonic and Vibro-Acoustical Techniques for Nondestructive Evaluation, *Taylor and Francis* (2019).

[13] C. Wong, W. Zhang, S. Lau, Periodic forced vibration of unsymmetrical piecewise-linear systems by incremental harmonic balance method, *Journal of Sound and Vibration*, 149(1) (1991) 91–105.

[14] Y. Chu, M. Shen, Analysis of forced bilinear oscillators and the application to cracked beam dynamics, *AIAA Journal*, 30(30) (1992) 2512–2519.

[15] S. Chatterjee, A. Mallik, A. Ghosh, Periodic response of piecewise non-linear oscillators under harmonic excitation, *Journal of Sound and Vibration*, 191(1) (1996) 129–144.

[16] A. Rivola, P. White, Bispectral analysis of the bilinear oscillator with application to the detection of fatigue cracks, *Journal of Sound and Vibration*, 216(5) (1998) 889–910.

[17] S. Cheng, A. Swamidas, X. Wu, A. Swamidas, Vibrational response of a beam with a breathing crack, *Journal of Sound and Vibration*, 225(1) (1999) 201–208.

[18] J. Ji, C. Hansen, On the approximate solution of a piecewise nonlinear oscillator under super-harmonic resonance, *Journal of Sound and Vibration*, 283(1-2) (2005) 467–474.

[19] A. Bovsunovskii, C. Surace, O. Bovsunovskii, The effect of damping and force application point on the non-linear dynamic behavior of a cracked beam at sub-and superresonance vibrations, *Strength of Materials*, 38(5) (2006) 492–497.

[20] L. Gelman, S. Gorpinich, C. Thompson, Adaptive diagnosis of the bilinear mechanical systems, *Mechanical Systems and Signal Processing*, 23(5) (2009) 1548–1553.

[21] A. Chatterjee, Structural damage assessment in a cantilever beam with a breathing crack using higher order frequency response functions, *Journal of Sound and Vibration*, 329(16) (2010) 3325–3334.

[22] W. Liu, M. Barkey, Nonlinear vibrational response of a single edge cracked

beam, *Journal of Mechanical Science and Technology*, 31(11) (2017) 5231–5243.

[23] R. Ruotolo, C. Surace, P. Crespo, D. Storer, Harmonic analysis of the vibrations of a cantilevered beam with a closing crack, *Computers and Structures*, 61(6) (1996) 1057–1074.

[24] N. Pugno, C. Surace, R. Ruotolo, Evaluation of the non-linear dynamic response to harmonic excitation of a beam with several breathing cracks, *Journal of Sound and Vibration*, 235(5) (2000) 749–762.

[25] K. Sholeh, A. Vafai, A. Kaveh, Online detection of the breathing crack using an adaptive tracking technique, *Acta Mechanica*, 188(3-4) (2007) 139–154.

[26] A. Bouboulas, N. Anifantis, Finite element modeling of a vibrating beam with a breathing crack: observations on crack detection, *Structural Health Monitoring-An International Journal*, 10(2) (2010) 131–145.

[27] P. Casini, F. Vestroni, Characterization of bifurcating non-linear normal modes in piecewise linear mechanical systems, *International Journal of Non-Linear Mechanics*, 46(1) (2011) 142–150.

[28] O. Giannini, P. Casini, F. Vestroni, Non-linear harmonic identification of breathing cracks in beams, *Computers and Structures*, 129 (2013) 166–177.

[29] W. Nan, Study of forced vibration response of a beam with a breathing crack using iteration method, *Journal of Mechanical Science and Technology*, 29(7) (2015) 2827–2835.

[30] F. Dotti, V. Cortínez, F. Reguera, Non-linear dynamic response to simple

harmonic excitation of a thin-walled beam with a breathing crack, *Applied Mathematical Modelling*, 40(1) (2015) 451–467.

[31] M. Shen, Y. Chu, Vibrations of beams with a fatigue crack, *Computers and Structures*, 45(1) (1992) 79–93.

[32] A. Chasalevris, C. Papadopoulos, A continuous model approach for cross-coupled bending vibrations of a rotor-bearing system with a transverse breathing crack, *Mechanism and Machine Theory*, 44(6) (2009) 1176–1191.

[33] S. Caddemi, I. Caliò, M. Marletta, The non-linear dynamic response of the Euler – Bernoulli beam with an arbitrary number of switching cracks, *International Journal of Non-Linear Mechanics*, 45(7) (2010) 714–726.

[34] M. Rezaee, R. Hassannejad, A new approach to free vibration analysis of a beam with a breathing crack based on mechanical energy balance method, *Acta Mechanica Solida Sinica*, 24(2) (2011) 185–194.

[35] H. Lim, H. Sohn, P. Liu, Binding conditions for nonlinear ultrasonic generation unifying wave propagation and vibration, *Applied Physics Letters*, 104(21) (2014) 315–326.

[36] K. Wang, M. Liu, Z. Su, Analytical insight into “breathing” crack-induced acoustic nonlinearity with an application to quantitative evaluation of contact cracks, *Ultrasonics*, 88 (2018) 157–167.

[37] A. Leissa, M. Qatu, Vibration of continuous systems, *McGraw Hill*, 2011.

[38] H. Xu, L. Cheng, Z. Su, J. Guyader, Identification of structural damage based on locally perturbed dynamic equilibrium with an application to beam

component, *Journal of Sound and Vibration*, 330 (2011) 5963–5981.

[39] M. Cao, L. Cheng, Z. Su, H. Xu, A multi-scale pseudo-force model in wavelet domain for identification of damage in structural components, *Mechanical Systems and Signal Processing*, 28 (2012) 638–659.

[40] M. Cao, Z. Su, L. Cheng, H. Xu, A multi-scale pseudo-force model for characterization of damage in beam components with unknown material and structural parameters, *Journal of Sound and Vibration*, 332 (2013) 5566–5583.

[41] H. Xu, Z. Su, L. Cheng, J. Guyader, P. Hamelin, Reconstructing interfacial force distribution for identification of multi-debonding in steel-reinforced concrete structures using noncontact laser vibrometry, *Structural Health Monitoring-An International Journal*, 12(5-6) (2013) 507–521.

[42] H. Xu, L. Cheng, Z. Su, J. Guyader, Damage visualization based on local dynamic perturbation: Theory and application to characterization of multi-damage in a plane structure, *Journal of Sound and Vibration*, 332 (2013) 3438–3462.

[43] H. Xu, L. Cheng, Z. Su, Suppressing influence of measurement noise on vibration-based damage detection involving higher-order derivatives, *Advances in Structural Engineering*, 16 (1) (2013) 233-244.

[44] H. Xu, Z. Su, L. Cheng, J. Guyader, A “Pseudo-excitation” approach for structural damage identification: From “Strong” to “Weak” modality, *Journal of Sound and Vibration*, 337 (2015) 181–198.

[45] H. Xu, B. Lu, Z. Su, L. Cheng, Statistical enhancement of a dynamic

equilibrium-based damage identification strategy: Theory and experimental validation, *Journal of Sound and Vibration*, 351 (2015) 236–250.

[46] C. Zhang, L. Cheng, H. Xu, J. Qiu, Structural damage detection based on virtual element boundary measurement, *Journal of Sound and Vibration*, 372 (2016) 133-146.

[47] H. Xu, Z. Su, L. Cheng, J. Guyader, On a hybrid use of structural vibration signatures for damage identification: a virtual vibration deflection (VVD) method, *Journal of Vibration and Control*, 23(4) (2017) 615-631.

[48] H. Xu, Q. Zhou, M. Cao, Z. Su, Z. Wu, A dynamic equilibrium-based damage identification method free of structural baseline parameters experimental validation in a two-dimensional plane structure, *Journal of Aerospace Engineering*, 31(6) (2018) 04018081.

[49] C. Zhang, H. Ji, J. Qiu, L. Cheng, W. Yao, Y. Wu, A local specific stiffness identification method based on a multi-scale “weak” formulation, *Mechanical Systems and Signal Processing*, 2020, 140: 106650.

[50] Z. Su, L. Ye, Lamb wave propagation-based damage identification for quasi-isotropic CF/EP composite laminates using artificial neural algorithm: Part II - Implementation and validation, *Journal of Intelligent Material Systems and Structures*, 2005, 16(2): 113-125.

[51] F. Li, G. Meng, K. Kageyama, Z. Su, L. Ye, Optimal mother wavelet selection for lamb wave analyses, *Journal of Intelligent Material Systems and Structures*, 2009; 20(10): 1147-1161.

[52] M. Cao, W. Ostachowicz, M. Radzieński, W. Xu. Multiscale shear-strain gradient for detecting delamination in composite laminates. *Applied Physics Letters*, 2013; 103: 101910.

[53] W. Xu, H. Fang, M. Cao, L. Zhou, Q. Wang, W. Ostachowicz, A noise-robust damage indicator for characterizing singularity of mode shapes for incipient delamination identification in CFRP laminates, *Mechanical Systems and Signal Processing*, 2019, 121: 183-200.

[54] W. Xu, Z. Su, J. Liu, M. Cao, W. Ostachowicz, Singular energy component for identification of initial delamination in CFRP laminates through piezoelectric actuation and non-contact measurement, *Smart Materials and Structures*, 2020, 29: 045001.

[55] M. Cao, Z. Su, Hao Xu, M. Radzieński, W. Xu, W. Ostachowicz, A novel damage characterization approach for laminated composites in the absence of material and structural information, *Mechanical Systems and Signal Processing*, 2020, 143: 106831.